

Interactions of quadrupolar nematic colloids

M. Škarabot,¹ M. Ravnik,² S. Žumer,^{1,2} U. Tkalec,¹ I. Poberaj,² D. Babič,² N. Osterman,² and I. Muševič^{1,2}

¹*J. Stefan Institute, Jamova 39, 1000 Ljubljana, Slovenia*

²*Faculty of Mathematics and Physics, University of Ljubljana, Jadranska 19, 1000 Ljubljana, Slovenia*

(Received 9 January 2008; published 24 March 2008)

We present experimental and theoretical study of colloidal interactions in quadrupolar nematic liquid crystal colloids, confined to a thin planar nematic cell. Using the laser tweezers, the particles have been positioned in the vicinity of other colloidal particles and their interactions have been determined using particle tracking video microscopy. Several types of interactions have been analyzed: (i) quadrupolar pair interaction, (ii) the interaction of an isolated quadrupole with a quadrupolar chain, and (iii) the interaction of an isolated quadrupolar colloidal particle with a two-dimensional (2D) quadrupolar crystallite. In all cases, the interactions are of the order of several $100k_B T$ for $2\ \mu\text{m}$ particles, which gives rise to relatively stable 2D colloidal crystals. The experimental results are compared to the predictions of Landau–de Gennes theory and we find a relatively good qualitative agreement.

DOI: [10.1103/PhysRevE.77.031705](https://doi.org/10.1103/PhysRevE.77.031705)

PACS number(s): 61.30.-v, 64.70.pv

I. INTRODUCTION

Nematic colloids are dispersions of solid, liquid, or gaseous particles in nematic liquid crystals. The first experiments on nematic colloids have been reported in the seventies, where foreign particles have been introduced into the nematic liquid crystal in order to observe the direction of the molecular alignment at the nematic-air interface [1,2]. It has been found that foreign particles spontaneously assembled into chains, which were all aligned-up along the average direction of the orientation of the liquid crystalline molecules at the interface. The ordering of the nematic liquid crystal could therefore be visualized via “decoration” of the nematic liquid crystal by chains of particles, very similar to the visualization of domains in solid ferroelectrics or ferromagnetics.

The interest in the spontaneous assembly of particles has been revived by Poulin *et al.* [3,4], who identified the fundamental role of topology and topological defects in the mechanism of formation of nematic colloidal chains. This has been followed by a great number of theoretical and experimental studies on nematic colloids and their interactions [5–23]. Recently, it has been reported that nematic colloids do not only spontaneously form one-dimensional (1D) chains, but also highly ordered and robust 2D nematic colloidal crystals [24]. This has opened an entirely new area of colloidal research with a possibility to create novel colloidal materials, which cannot be made in water-based colloidal systems. In contrast to the traditional colloidal dispersions, where the interactions between colloidal particles are mediated by the forces of electromagnetic origin, the interactions in the nematic colloids are mediated by the elasticity of the distorted nematic liquid crystal around the dispersed particles. These effective interactions are anisotropic in their nature and result in far more complex colloidal crystalline structures compared to the water-based colloidal systems.

When a small colloidal particle, such as a microsphere made of glass, silica, polymer, etc., is immersed in the nematic liquid crystal, the surface of the particle interacts with liquid crystalline molecules and forces them to align into a preferred direction relative to the surface. This surface-

induced order creates distortion of the nematic around the particle, which spreads over macroscopic distances and the particle appears much larger than its actual size. The distortion of the nematic liquid crystal around the inserted colloidal particle is anisotropic, even though the particle itself is spherical. The reason for this is creation of topological defects in the nematic liquid crystal, which inevitably appear whenever the particle is inserted into the liquid crystal. These defects are in a form of topological point defects or small loops, which are located in the vicinity of the particle’s surface and cannot be separated from the particle, or annihilated. The reason for this is the fundamental law of conservation of the topological charge, which is associated with topological defects [25]. The law of conservation of the topological charge is very much alike the law of conservation for the total electric charge in electrostatics and bears many similarities.

Within a more detailed description, the topological defects appear in a form of a point defect [4,9,10] (radial and hyperbolic hedgehog), or in a form of a small disclination ring [9,26,27], both carrying the topological charge of magnitude 1. The type of the defect depends on the size of the colloidal particle and strength of surface anchoring [26,28], size of the particle [29], and can be even transformed one into another by changing the surface anchoring or exerted confinement [9,30]. When the colloidal surface favors homeotropic surface anchoring, there are two possible configurations or shapes of the distorted nematic around the colloidal particle. In the first type, the colloidal particle is accompanied by a hyperbolic hedgehog defect, whereas the particle itself can be considered as a source of the radial hedgehog defect, which is located in its center. Together they form a topological pair, reminiscent of an electric dipole, hence such a configuration is called a topological dipole. In the second configuration, the defect appears in a form of a large disclination ring, that encircles the colloidal particle and is called the Saturn ring. The symmetry of this configuration is quadrupolar, hence we are describing these type of colloids as quadrupolar nematic colloids. An example of quadrupolar colloidal particles with a defect in a form of a Saturn ring is presented in Fig. 1.

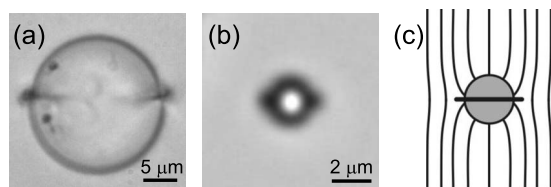


FIG. 1. (a) A Saturn ring is clearly visible when larger colloidal particles with homeotropic surface anchoring are observed in a planar nematic cell under an optical microscope. (b) With smaller microspheres, the ring is barely observed and appears in a form of two dark spots. (c) Schematic drawing of the director field around Saturn-like colloidal particle.

When several colloidal particles are brought together in the nematic liquid crystal, their regions of distortion start to overlap. This means that the total energy of the system depends on particle separation, and a force of structural origin emerges between the particles. It has been shown that the structural forces between colloidal inclusions in liquid crystals lead to a diversity of self-assembled structures, including colloidal crystals in 2D.

The purpose of this paper is to present a detailed and complete experimental and theoretical study of the interactions between quadrupolar nematic colloids, although they have been studied before by other authors. In the experimental part we describe in detail the sample preparation and experimental procedures, which is followed by the presentation of different types of quadrupolar interactions: quadrupolar pair interaction leading to the formation of linear, chainlike colloidal structures, and the assembly of quadrupolar 2D colloidal crystalline structures. The theoretical section describes the Landau–de Gennes (LdG) approach to the analysis of forces between quadrupolar colloids and stability of colloidal assemblies in 1D and 2D. The paper concludes with a brief discussion of observed phenomena.

II. EXPERIMENT

Silica spheres of diameter $2R=(2.32 \pm 0.03) \mu\text{m}$ and $4.7 \mu\text{m}$, with the refractive index $n_s=1.37$, have been used in all experiments. The surface of the silica spheres was first covered with a monolayer of *N,N*-dimethyl-*N*-octadecyl-3-aminopropyl trimethoxysilyl chloride (DMOAP), which ensures a very strong homeotropic surface anchoring of a nematic liquid crystal. This surface functionalization was performed by first immersing colloidal microspheres into 1% water solution of DMOAP for a period of 5 min. After that, the dispersion was put in a centrifuge to sediment the microspheres at the bottom of the container. The DMOAP solution was then removed, pure water was added and the dispersion was again sedimented using centrifugal force. This procedure of removing remaining DMOAP was repeated several times. After drying, the colloidal particles were dispersed in the nematic liquid crystal pentylcyanobiphenyl (5CB) at a typical concentration of 1%. The surfaces of colloidal microspheres, which were treated with DMOAP, are known to induce strong perpendicular orientation of the nematic. The cells were assembled of two

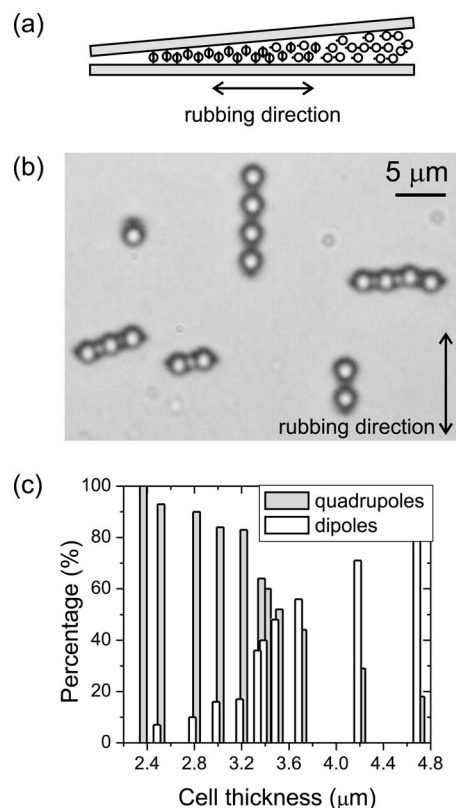


FIG. 2. (a) Schematics: in thinner parts of a planar wedge-type nematic cell, the particles with homeotropic surface anchoring are of quadrupolar symmetry. In thicker parts of the cell, dipolar colloids are observed. (b) At a critical cell thickness, both types of particles are observed. Dipolar colloids form linear chains, directed along the rubbing direction, whereas quadrupolar colloids form kinked chains, perpendicular to the rubbing direction. (c) Histogram presenting the number of dipolar and quadrupolar colloidal particles at different cell thickness. Note rather broad region of the coexistence of both colloidal types.

parallel optically transparent indium tin oxide (ITO) coated glasses. The ITO coating was used in order to increase the absorption of the laser light of the laser tweezers which could provide local melting of the nematic in some of the experiments. The planar anchoring on the two boundary glasses was obtained by rubbed polyimide coating. Wedge-type cells were used, with thickness in the range from 2 to $8 \mu\text{m}$, as measured by a standard interference technique before filling them with 5CB. The nematic colloidal dispersion was introduced into a thin planar cell with rubbed polyimide alignment layers using capillary force.

In our experiments, we have used the surface confinement of a very thin planar cell to select either dipolar or quadrupolar, i.e., Saturn ring configuration. As we have reported earlier, the colloidal particles were of dipolar symmetry in thicker parts of the wedgelike cell, as shown schematically in Fig. 2(a). During time, they spontaneously aggregate and form dipolar chains, as shown in Fig. 2(b). One can see that the dipolar chains are oriented along the rubbing direction of the cell, i.e., along the nematic director in planar nematic cell. In thinner parts of the cells, the colloidal particles were of quadrupolar symmetry. This can be considered as if the

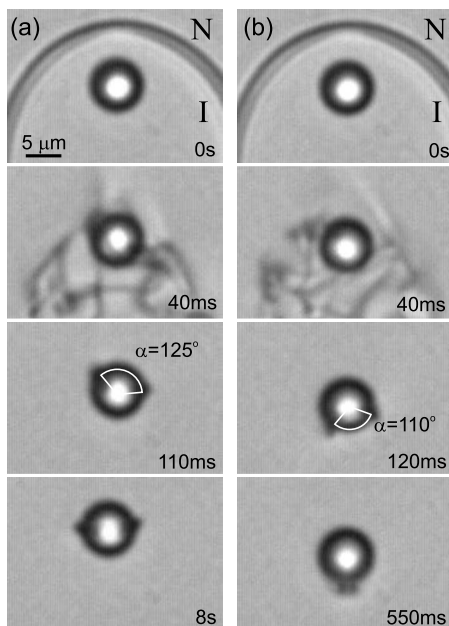


FIG. 3. When the cell thickness is close to the critical thickness h_c for the dipolar-to-quadrupolar transition, quenching a small isotropic island around a selected colloidal particle can result either in (a) quadrupolar colloidal structure or (b) dipolar colloidal structure. In this particular case the cell thickness was $7 \mu\text{m}$ and the diameter of the silica colloidal particles with DMOAP surface coating was $4.7 \mu\text{m}$.

tight planar confinement induces “opening” of a point defect into a ringlike defect, which encircles the colloidal particle. The transition from the dipolar to the quadrupolar colloids could be clearly visible under the microscope and is illustrated in Fig. 2(b), where the coexistence of both types can be observed. Some of the colloidal particles form dipolar colloidal chains, oriented along the rubbing direction, whereas the others are quadrupoles and form kinked chains, oriented perpendicular to the rubbing direction.

We have analyzed the transition from the dipolar to the quadrupolar colloidal structure as a function of local thickness in wedgelike planar nematic cells by counting the number of dipolar and quadrupolar colloidal particles at a chosen thickness. The distribution of both colloidal types is shown in Fig. 2(c). In this particular case, the critical thickness for DMOAP coated $2.32 \mu\text{m}$ silica particles was $h_c=3.5 \mu\text{m}$. The distribution is rather broad and the coexistence region corresponds to a variation of the local thickness of $\sim 1 \mu\text{m}$.

The metastability and coexistence of dipolar and quadrupolar colloidal states at the critical cell thickness are nicely illustrated in an experiment shown in Fig. 3, where the nematic liquid crystal is quenched from the isotropic into the nematic phase, and the cell thickness is around the critical thickness h_c . Using high power of the laser tweezers we have locally heated the nematic liquid crystal, so that the colloidal particle was surrounded by a small island of the isotropic melt. Then the laser was switched-off and the isotropic melt rapidly cooled across the isotropic-nematic transition. The results of these quench experiments are shown in Fig. 3. In a fraction of a second after switching-off the laser, a disordered

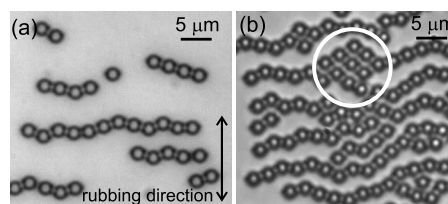


FIG. 4. A majority of self-assembled quadrupolar colloidal structures are just kinked chains, shown in (a). However, in some parts of the sample, spontaneously ordered 2D quadrupolar crystallites are observed, such as the one in the encircled region in (b).

nematic region appears, which is filled with entangled line defects. These annihilate and a single topological defect remains, either in a form of a small ring, encircling the colloidal particle, or in a form of a point defect. Each of these states appears with a roughly equal probability, and the emergence of a state depends on the angle α , specifying the “opening” of the topological defect loop immediately after the dense tangle of defects clears and only a single defect loop is present. If this angle is larger than $\alpha > 125^\circ$, the resulting state is quadrupolar, and if $\alpha < 110^\circ$, the final state is dipolar. This is valid for the particular colloidal particle and particular thickness and may vary from particle to particle.

Our investigations have been concentrated on the spontaneous and directed assembly of quadrupolar nematic colloidal particles, which could be observed below the critical thickness in our wedge-type cells. Careful inspections of as prepared samples reveals some interesting structures, formed spontaneously during the filling of the cells with nematic colloids. Figure 4 shows some typical colloidal structures, observed at a low density of colloidal particles, where the dominating majority of structures are just quadrupolar kinked chains. However, in some cases, one could clearly see quasicrystalline areas, such as the encircled area in the center of Fig. 4(b). This is a strong indication, that 2D quadrupolar nematic colloidal crystals could be assembled. In order to understand the interactions of quadrupolar colloidal particles in 2D, we have systematically investigated the nature of the interactions between quadrupolar colloidal particles.

We have first analyzed the interaction between an isolated quadrupolar colloidal particle and a kinked colloidal chain. Using the laser tweezers [31], individual colloidal particles have been trapped and positioned close to the selected colloidal chain, as shown in the first two images of Figs. 5(a) and 5(b). The colloidal particles were then released, so that they approached along the chain direction, as illustrated in Fig. 5. We have found that there are two “easy” directions for the colloidal binding to the already formed quadrupolar colloidal chain. Each of these directions forms an angle of $\approx 17^\circ$ with respect to the “average” chain direction, which is itself perpendicular to the rubbing direction. In the first scenario, illustrated in the sequence of images in Fig. 5(a), the colloidal particles formed a kinked quadrupolar colloidal chain, with alternating directions of sequent colloidal particles, as already reported earlier. Alternatively, straight quadrupolar colloidal chains could be assembled, which were tilted with

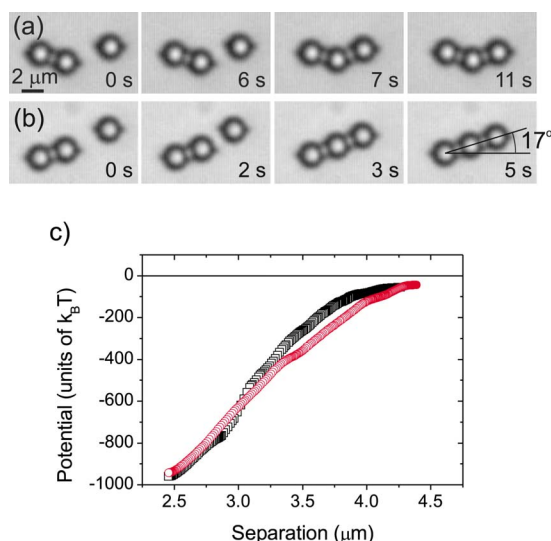


FIG. 5. (Color online) Quadrupolar colloidal chains can grow in a form of kinked (a) or straight chains (b). (c) The quadrupole-quadrupole interaction, as a function of separation between the particle and the closest particle in the chain. The squares correspond to a , the circles correspond to b .

respect to the rubbing direction, as shown in Fig. 5(b). In both cases, the binding energy is of the order of $1000k_B T$, as illustrated in Fig. 5(c). For details on the experimental technique, which was used to determine the interaction potentials see Refs. [31–36]

The nematic colloidal quadrupoles do not only form chains, but they also tend to form 2D regular patterns, as illustrated in Fig. 6. Here, an isolated quadrupole was positioned close to the kinked chain and released. One can see, that when the additional quadrupole is incorporated into the

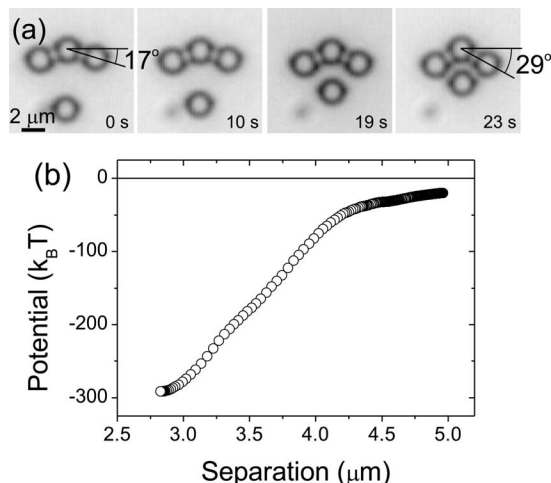


FIG. 6. (a) An isolated quadrupolar colloidal particle is attracted laterally to the already formed quadrupolar chain. Note that the chain is slightly distorted after inclusion of an extra particle, as the “kink” angle increases from 17° to 29° . (b) The lateral quadrupolar interaction is weaker and amounts only to $\sim 1/3$ of the head-to-head quadrupolar interaction. The binding of quadrupoles in 2D quadrupolar colloidal crystals is therefore highly anisotropic.

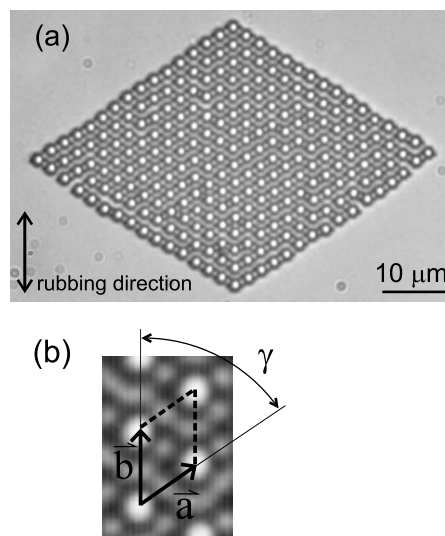


FIG. 7. (a) Large scale quadrupolar nematic colloidal crystals could be assembled using laser tweezers. (b) The unit cell of the quadrupolar nematic colloidal crystal is oblique. The lattice vectors for $2.32 \mu\text{m}$ colloidal particles in a $2.7 \mu\text{m}$ planar cell are $a = (2.69 \pm 0.04) \mu\text{m}$, $b = (3.01 \pm 0.05) \mu\text{m}$, and $\gamma = (56 \pm 1)^\circ$.

2D crystallite, the angles between “colloidal bonds” change significantly. Although the interaction is in this case only $\sim 1/3$ of the head-to-head approach, see Fig. 6(b), it is still significant and drives colloidal assembly in 2D quadrupolar crystallites. It is important to note the significance of this observation, as it allows us to assemble using laser tweezers larger scale 2D quadrupolar nematic colloidal crystals, similar to the one shown in Fig. 7(a).

Although assembling hundreds of particles using laser tweezers is time consuming (it may take a day to assemble a crystal, shown in Fig. 7), it clearly shows an important principle, that large scale 2D colloidal crystals could, in principle, be built. The high anisotropy between the “head-to-head” and “lateral” quadrupolar colloidal binding is evident by the naked eye from Fig. 7(a). One can easily see that when building a quadrupolar crystal, it is difficult to avoid completely the “memory effects” from the assembly procedure. Namely, when assembling the crystal from chains or particles, not always a complete restructuring to a crystallite occurs and thus some irregularities pertain in the crystalline lattice. The analysis of the unit cell of a quadrupolar colloidal crystal [Fig. 7(b)] shows that it is an oblique one, corresponding to a slightly distorted hexagonal order. The angle γ between the lattice vectors is $(56 \pm 1)^\circ$.

The high anisotropy of the quadrupole to particle interaction is responsible also for the fragility of 2D quadrupolar nematic colloidal crystals. They are quite susceptible to external perturbations, such as the change of temperature and temperature gradients, which tend to generate macroscopic flow of the nematic crystals. If special precautions are not taken into account, a gradual deterioration of the 2D order occurs, which is illustrated in Fig. 8. One can see that individual quadrupolar chains have been detached from the rest of the crystallite, as the interaction between neighboring chains (straight or kinked) is much less than the binding along the chain.

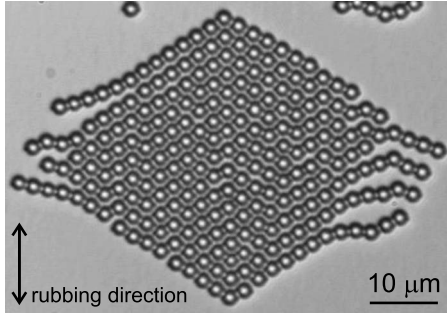


FIG. 8. Unlike the dipolar interaction [22], the quadrupolar interaction, especially lateral, is not sufficient to resist the external perturbations, such as the change of temperature and the flow of the liquid crystal. This results to gradual (over a month period) decomposition of the order.

III. THEORY

Quadrupolar colloidal structures were theoretically investigated using the Landau–de Gennes free energy minimization approach [2]. Here, a free energy functional F is constructed phenomenologically from the tensorial order parameter Q_{ij} , which is joining together three main properties of the nematic colloids: (i) nematic elasticity, (ii) possible formation of the defects, and (iii) surface interaction between the nematic and colloidal particles. As the free energy F typically cannot be minimized analytically in complex geometries, a numerical relaxation algorithm was used to solve the governing bulk and surface Euler-Lagrange equations [35]

$$L\nabla^2 Q_{ij} - A Q_{ij} - B Q_{ik} Q_{kj} - C Q_{ij} (Q_{kl} Q_{lk}) = 0, \quad (1)$$

$$L \frac{\partial Q_{ij}}{\partial x_k} \nu_k + W(Q_{ij} - Q_{ij}^0) = 0. \quad (2)$$

Here L is a single elastic constant, A , B , and C are the bulk nematic material parameters, W is the surface anchoring parameter, ν_k is the particle surface normal, and Q_{ij}^0 is a preferred surface order parameter tensor determining both the surface orientation and the magnitude of the order. The parameters corresponding to a 5CB nematic liquid crystal and a strong surface anchoring have been used in the calculations: $L = 4.0 \times 10^{-11}$ N, $A = -0.172 \times 10^6$ J/m³, $B = -2.12 \times 10^6$ J/m³, $C = 1.73 \times 10^6$ J/m³, and $W = 1.0 \times 10^{-2}$ J/m².

We have recently reported [37] that there are basically two distinct mechanisms of colloidal binding in thin nematic cells. (i) Binding by localized topological defects in a form of points or loops. In this case, the defects are localized to a single colloidal particle, see, for example, Ref. [24]. (ii) Binding by entangled topological defects [37]. In this case, the defects appear in a form of extended topological defect loop, winding-up around several colloidal particles and binding them together.

We have shown that by choosing proper initial configurations of the order parameter tensor profile in the relaxation algorithm, one can introduce into a colloidal system a large degree of disorder, which naturally leads to the formation of

different metastable entangled defect states. As these complicated entangled states are not of interest in the present paper, and we want to avoid them, all calculations were started from a uniform initial tensor configuration, corresponding to a uniform spatially independent director field \vec{n} . We observe that by starting from a uniform orientation, a Saturn ring defect gradually starts to form at the equator of the particle in the plane perpendicular to \vec{n} at the very beginning of our calculations. The defect first lies at the surface of the particle, but if the anchoring is strong enough, then the defect relatively quickly (within few 100 explicit iteration steps) detaches from the surface and forms a real ring. By changing the initial uniform orientation of the director field \vec{n} around a chosen particle, one can also control the initial orientation of the Saturn ring defect, as it always lies in the plane perpendicular to \vec{n} .

Before discussing the interactions between quadrupolar nematic colloids, let us briefly discuss the experimentally observed transition from a dipolar to the quadrupolar nematic configuration around a single colloidal particle. This observation invites the interesting question of whether the “intermediate” defect, or director field configuration with only a partly opened defect ring, is stable. Whereas in the experiments only two stable configurations were observed (see Figs. 2 and 3), there is no inherent theoretical constraint why there could not exist a “combined dipolar-quadrupolar” configuration. In this intermediate case, a hyperbolic point defect could be partly open and could form a ring at a nonzero latitude of the colloidal particle. To address this question more precisely, we have performed a set of numerical calculations, each starting from a predetermined initial tensor field condition mimicking an intermediate partly opened defect configuration, and then followed the stability of the selected structure.

We have started our numerical relaxation calculations using the dipolar director far-field ansatz [9] $\vec{n} = \hat{e} + qR^2 \vec{r}/r^3$. In this ansatz, \hat{e} is a unit vector, which determines the far-field orientation of the nematic and \vec{r} is a position vector from the colloidal particle placed at $\vec{r} = 0$. By changing the numerical constant q , one can vary the initial size of the disclination ring of the hyperbolic defect [35]. The parameter q is thus closely related to the experimentally introduced opening angle (Sec. II and Fig. 3). The numerical constant equals $q = 3.08$ for an equilibrium dipolar configuration and fixes the position of the hyperbolic defect at the distance $1.17R$ from the center of the particle [9]. By taking a smaller q , one demands that the defect forms closer to the particle and for small enough q , a virtual defect is formed even inside the particle. In the latter case, this effectively results in the formation of a partly opened defect ring at a particle latitude, which depends on q . In the limit of $q = 0$ the initial condition becomes actually $\vec{n} = \hat{e}$, which is a uniform director field, and the defect ring forms at the particle equator, as already commented in the previous paragraph.

Figure 9 (upper four frames) shows several initial nematic configurations for different numerical constants q . In these images, the snapshots of the director field profile and the scalar order parameter were taken after only 100 iterative steps, which can be considered as the beginning of the calculation, since the final equilibrium relaxed state is reached

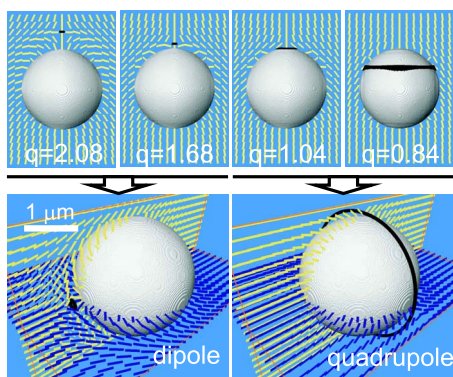


FIG. 9. (Color online) Numerical study of a dipolar to quadrupolar defect transition. The upper four frames show the initial configurations of the director field, which are different in the position and size of the defect ring. Initial configurations with $q \geq 1.68$ relax into the final dipolar configuration, shown in lower left image, and the starting configurations with $q \leq 1.04$ relax into the quadrupolar state, shown in the lower right image. The defects are visualized in black, corresponding to isosurfaces of $S=0.48$ (compared to $S_{\text{bulk}}=0.533$). The numerical parameters: the colloidal particle diameter $2R=2.0 \mu\text{m}$ and the cell thickness $h=2.5 \mu\text{m}$.

after ~ 100000 steps. One can see that by taking different starting q 's, one can nicely predetermine the initial diameter of the defect ring, as well as the corresponding starting director field. Interestingly, our calculations clearly show only two final equilibrium relaxed states, namely the elastic dipole and the elastic quadrupole. We should stress, that this is in full agreement with experiments, where no intermediate configurations were observed. For the initial conditions with $q \geq 1.68$, the corresponding configuration relaxes into the dipolar state (Fig. 9, lower left). On the other hand, by choosing lower values of $q \leq 1.04$, the stable final state is the quadrupolar structure (Fig. 9, lower right). We should comment that the dipolar structure is less stable and already a smaller perturbation of the dipole, i.e., a smaller effective opening angle α , triggers a transformation into the quadrupole.

Focusing on the stability of two-dimensional quadrupolar structures, we have first studied the stability of a kinked quadrupolar trimer and a quadrupolar rhomb. Both can be understood as a building block of a larger quadrupolar 2D colloidal crystal. It is therefore interesting to observe possible changes in the equilibrium particle configurations, since these will be directly reflected in the unit cell of the larger 2D crystallite.

The results for the kinked quadrupolar colloidal trimer are shown in Fig. 10. The equilibrium kink angle $\beta^{\text{trimer}} = \arctan(Y^{\text{eq}}/X^{\text{eq}})$ is numerically found to be 13.4° , and the binding potential is of the order of $\sim 1000k_B T$ per “quadrupolar bond.” Both values are in good agreement with the experiments ($\beta_{\text{exp}}^{\text{trimer}}=17^\circ$, $\sim 1000k_B T$ binding potential).

When an additional particle is added to the trimer to build a rhombic quadmer (Fig. 11) indeed the configuration and the kink-angle change profoundly to $\beta^{\text{rhomb}}=31.7^\circ$ as observed in the experiments ($\beta_{\text{exp}}^{\text{rhomb}}=29^\circ$). When looking at the trimer and quadmer equilibrium configurations, it is interesting to notice, how the Saturn rings unbend in the quadmer

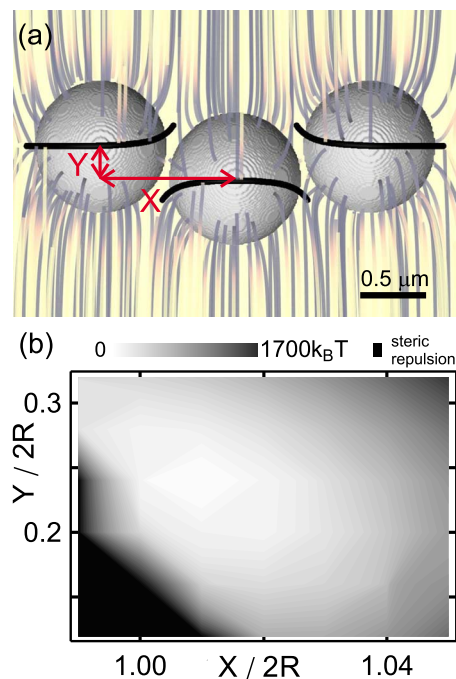


FIG. 10. (Color online) (a) A kinked quadrupolar colloidal trimer in the equilibrium configuration. Defect rings in black are visualized as isosurfaces of the scalar order parameter $S=0.48$ ($S_{\text{bulk}}=0.533$); streamlines show the corresponding director field profile. (b) Binding potential for stretching of the kinked trimer. Numerical parameters: colloidal particle diameter $2R=1.0 \mu\text{m}$ and cell thickness $h=1.4 \mu\text{m}$.

configuration. Such a behavior of defect rings can indeed be seen from the experiments, if one carefully studies Figs. 5(a) and 6(a) (note the positions of the dark spots at the sides of the particles). The effect of the cell thickness on the equilibrium particle configuration was evaluated for both trimer and quadmer structures. For the kinked trimer, we observe that by increasing the cell thickness from 1.4 to $2.0 \mu\text{m}$, the kink angle β^{trimer} decreases from 13.4° to 11.1° , whereas for the rhombic quadmer β^{rhomb} it increases slightly from 31.7° to 32.2° .

Finally, we emphasize in more detail the stability of a two-dimensional quadrupolar colloidal crystal, which has already briefly been presented before [24]. The director field profile in a cross-section parallel to the cell walls and the corresponding topological defects are shown in Fig. 12. Here, the periodic boundary conditions have been used in the x and y directions, forming a rectangular unit cell of a total of two particles. The boundary conditions on top and bottom of the cell have been fixed uniform. In principle the symmetry of the quadrupolar crystal would also allow a smaller rhombic unit cell with a total of one particle, however, for programming reasons it was simpler to implement the rectangular cell to our numerical finite difference relaxation algorithm. Recalling that the equilibrium “kink angle” of the two-dimensional crystal was 35° [24] and comparing it to the kink angle of the rhombic quadmer $\beta^{\text{rhomb}}=32.2^\circ|_{h=2 \mu\text{m}}$, one can see that the quadmer can indeed be considered as a progenitor of the 2D crystalline colloidal ordering since it

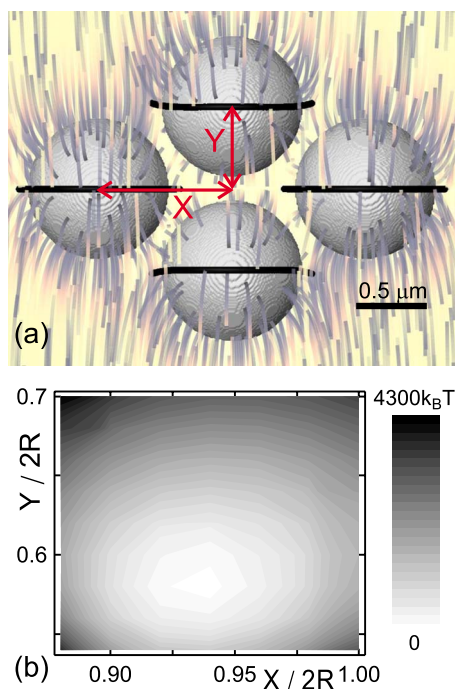


FIG. 11. (Color online) (a) A quadrupolar colloidal rhomb: defect rings are colored black, corresponding to isosurfaces of $S = 0.48$, whereas the streamlines visualize the director field. (b) The binding potential for stretching of the rhomb particle configuration. Note that the binding energy is $\sim 1000k_B T$ per particle. The numerical parameters: the colloidal particle diameter $2R = 1.0 \mu\text{m}$, the cell thickness $h = 1.4 \mu\text{m}$.

predetermines the basic particle positioning which then further spans over the colloidal crystallite. The unit cell of the stable 2D quadrupolar colloidal crystal was oblique, with lattice constants of $a = 2.3R$ and $b = 2.64R$, with $\gamma = 55^\circ$, where γ is the angle between the two lattice vectors. These values are in qualitative agreement with experiments.

IV. CONCLUSIONS

Although quadrupolar interactions in nematics have been studied before, we have considered that it is important to present a detailed, complete and systematic study of quadru-

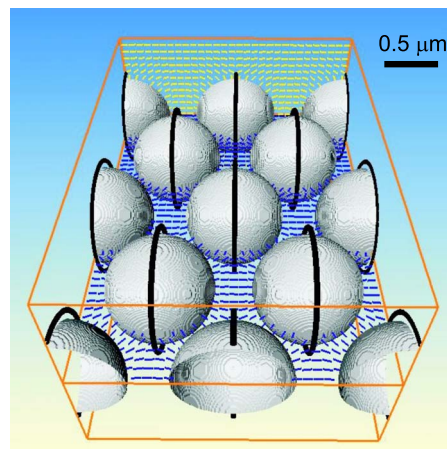


FIG. 12. (Color online) A numerically simulated stable configuration of a two-dimensional quadrupolar colloidal crystal. The defect rings are visualized in black, corresponding to isosurfaces of $S = 0.48$. The director field in two perpendicular planes is shown. The numerical parameters are: the colloidal particle diameter is $2R = 1.0 \mu\text{m}$, and the cell thickness is $h = 2.0 \mu\text{m}$.

polar colloidal interactions in thin planar nematic cells. In this paper, we have presented a systematic experimental and theoretical analysis of quadrupolar nematic colloidal interactions, starting from a simple pair colloidal interaction, continuing to the interactions of many colloidal particles in chains (1D) and finishing with the interactions, which lead to the formation of quadrupolar 2D nematic colloidal crystals. In all cases, the particles, their surface treatment and the cell conditions were the same, which gives us the ability to systematically follow the evolution of interactions, when many particles are present. We have found, that the quadrupolar colloidal interactions could be well described using a fully tensorial LdG approach. We find that the quadrupolar colloidal interaction in thin planar nematic cells is anisotropic, and it is weaker compared to the dipolar nematic colloidal interaction [35]. As a result, the 2D quadrupolar nematic colloidal crystals are not so stable as dipolar, and are more susceptible to external perturbation. Nevertheless, in spite of reduced potential for application, the mere existence of quadrupolar 2D crystals adds an important contribution to our understanding of the mechanisms, which are responsible for spontaneous or directed assembly in nematic colloids.

-
- [1] P. E. Cladis and P. Pieranski, C. R. Seances Acad. Sci., Ser. B **273**, 275 (1971).
 [2] P. G. de Gennes and J. Prost, *The Physics of Liquid Crystals*, 2nd ed. (Oxford Science Publications, Oxford, 1993).
 [3] P. Poulin, V. A. Raghunathan, P. Richetti, and D. Roux, J. Phys. II **4**, 1557 (1994).
 [4] P. Poulin, H. Stark, T. C. Lubensky, and D. A. Weitz, Science **275**, 1770 (1997).
 [5] S. Ramaswamy, R. Nityananda, V. A. Raghunathan, and J. Prost, Mol. Cryst. Liq. Cryst. Sci. Technol., Sect. A **288**, 175 (1996).
 [6] V. A. Raghunathan, P. Richetti, D. Roux, F. Nallet, and A. K. Sood, Mol. Cryst. Liq. Cryst. Sci. Technol., Sect. A **288**, 181 (1996).
 [7] O. V. Kuksenok, R. W. Ruhwandl, S. V. Shiyanovskii, and E. M. Terentjev, Phys. Rev. E **54**, 5198 (1996).
 [8] R. W. Ruhwandl and E. M. Terentjev, Phys. Rev. E **55**, 2958 (1997).
 [9] H. Stark, Phys. Rep. **351**, 387 (2001).
 [10] T. C. Lubensky, D. Petey, N. Currier, and H. Stark, Phys. Rev. E **57**, 610 (1998).
 [11] P. G. Petrov and E. M. Terentjev, Langmuir **17**, 2942 (2001).

- [12] J. C. Loudet, P. Poulin, and P. Barois, *Europhys. Lett.* **54**, 175 (2001).
- [13] M. Yada, Jun Yamamoto, and H. Yokoyama, *Langmuir* **18**, 7436 (2002).
- [14] V. G. Nazarenko, A. B. Nych, and B. I. Lev, *Phys. Rev. Lett.* **87**, 075504 (2001).
- [15] A. B. Nych, U. M. Ognysta, V. M. Pergamenschchik, B. I. Lev, V. G. Nazarenko, I. Muševič, M. Škarabot, and O. D. Lavrentovich, *Phys. Rev. Lett.* **98**, 057801 (2007).
- [16] M. Zapotocky, L. Ramos, P. Poulin, T. C. Lubensky, and D. A. Weitz, *Science* **283**, 209 (1999).
- [17] S. P. Meeker, W. C. K. Poon, J. Crain, and E. M. Terentjev, *Phys. Rev. E* **61**, R6083 (2000).
- [18] J. Anderson, E. M. Terentjev, S. P. Meeker, J. Crain, and W. C. K. Poon, *Eur. Phys. J. E* **4**, 11 (2001).
- [19] P. Poulin, V. Cabuil, and D. A. Weitz, *Phys. Rev. Lett.* **79**, 4862 (1997).
- [20] M. Yada, Jun Yamamoto, and H. Yokoyama, *Phys. Rev. Lett.* **92**, 185501 (2004).
- [21] C. M. Noel, G. Bossis, A.-M. Chaze, F. Giulieri, and S. Lacis, *Phys. Rev. Lett.* **96**, 217801 (2006).
- [22] I. I. Smalyukh, O. D. Lavrentovich, A. N. Kuzmin, A. V. Kachynski, and P. N. Prasad, *Phys. Rev. Lett.* **95**, 157801 (2005).
- [23] J. Kotar, M. Vilfan, N. Osterman, D. Babič, M. Čopič, and I. Poberaj, *Phys. Rev. Lett.* **96**, 207801 (2006).
- [24] I. Muševič, M. Škarabot, U. Tkalec, M. Ravnik, and S. Žumer, *Science* **313**, 954 (2006).
- [25] M. Kleman and O. D. Lavrentovich, *Philos. Mag.* **86**, 4117 (2006).
- [26] O. Mondain-Monval, J. C. Dedieu, T. Gulik-Krzywicki, and P. Poulin, *Eur. Phys. J. B* **12**, 167 (1999).
- [27] Y. Gu and N. L. Abbott, *Phys. Rev. Lett.* **85**, 4719 (2000).
- [28] J. C. Loudet, P. Barois, P. Auroy, P. Keller, H. Richard, and P. Poulin, *Langmuir* **20**, 11336 (2004).
- [29] C. Völtz, Y. Maeda, Y. Tabe, and H. Yokoyama, *Phys. Rev. Lett.* **97**, 227801 (2006).
- [30] J. C. Loudet, O. Mondain-Monval, and P. Poulin, *Eur. Phys. J. E* **7**, 205 (2002).
- [31] I. Muševič, M. Škarabot, D. Babič, N. Osterman, I. Poberaj, V. Nazarenko, and A. Nych, *Phys. Rev. Lett.* **93**, 187801 (2004).
- [32] M. Škarabot, M. Ravnik, D. Babič, N. Osterman, I. Poberaj, S. Žumer, I. Muševič, A. Nych, U. Ognysta, and V. Nazarenko, *Phys. Rev. E* **73**, 021705 (2006).
- [33] B. Lev, A. Nych, U. Ognysta, S. B. Chernyshuk, V. Nazarenko, M. Škarabot, I. Poberaj, D. Babič, N. Osterman, and I. Muševič, *Eur. Phys. J. E* **20**, 215 (2006).
- [34] M. Škarabot, U. Tkalec, and I. Muševič, *Eur. Phys. J. E* **24**, 99 (2007).
- [35] M. Škarabot, M. Ravnik, S. Žumer, U. Tkalec, I. Poberaj, D. Babič, N. Osterman, and I. Muševič, *Phys. Rev. E* **76**, 051406 (2007).
- [36] I. Muševič and M. Škarabot, *Soft Matter* **4**, 195 (2008).
- [37] M. Ravnik, M. Škarabot, S. Žumer, U. Tkalec, I. Poberaj, D. Babič, N. Osterman, and I. Muševič, *Phys. Rev. Lett.* **99**, 247801 (2007).